Localized SERS

DOI: 10.1002/ange.200905389

Direct Evidence of High Spatial Localization of Hot Spots in Surface-Enhanced Raman Scattering**

Chang Chen, James Andell Hutchison, Francesca Clemente, Ronald Kox, Hiroshi Uji-I, Johan Hofkens, Liesbet Lagae, Guido Maes, Gustaaf Borghs, and Pol Van Dorpe**

Surface enhanced Raman scattering (SERS) is a powerful tool in molecular and biomolecular analysis, offering chemically specific detection with a sensitivity that has been extended to the single-molecule level.[1–3] It has been established that SERS is dominated by strong electromagnetic field enhancement near metallic nanostructures, and that surface plasmon coupling at the junctions or gaps between these structures creates 'hot spots' with the enormous enhancement necessary for high-sensitivity SERS detection.[4] An intrinsic and important property of the hot spot is its high spatial localization. Theoretical studies predict that the SERS enhancement factor can reduce by an order of magnitude only a few nanometers away from the junction between two metal nanospheres.[5] Experimentally, this means that a few analyte molecules within a hot-spot region will dominate the overall SERS intensity, despite of the much larger number of analyte molecules on the surrounding substrate that are also irradiated.[6] Understanding the spatial distribution of SERS hot spots is therefore critical, especially to facilitate the interpretation of single-molecule SERS data, and the experimental hallmarks (e.g. intensity fluctuations) and minimum enhancement factors required for single-molecule SERS are topics of current debate.[7,8]

In the past decade, the high spatial localization of electromagnetic field hot spots was predicted by numerous numerical calculations.[5,9,10] Scanning near-field optical microscopy[11] and electron energy-loss spectroscopy[12] were also used to study surface plasmon (SP) distribution profiles and thus indirectly demonstrate the high spatial localization of SERS hot spots. However, owing to the diffraction-limited detection of SERS photons and the difficulty of precise and local deposition of analytes onto substrates, direct investigations using SERS remained difficult.[13]

Tip-enhanced Raman spectroscopy has provided excellent experimental evidence of the high spatial resolution of hot spots near the tip region, using the tip itself to control the characteristics of the hot-spot region.[14,15] Atomic layer deposition of alumina[16] or molecular rulers[17] placed on top of Ag nanospheres were also employed to demonstrate the analyte distance dependence of SERS. In all these cases, an inverse power law dependence of intensity with increasing distance was observed, showing the near-field character of SERS. Recently, photoinduced hole burning of molecules on a film of Ag nanospheres[6] and oxygen plasma etching of molecules on a Ag nanocube dimer[18] both demonstrated the overwhelming contribution of a few analyte molecules directly at the hot spot to the overall SERS signal.

Nevertheless, the most direct method to map the spatial distribution of a SERS hot spot would be to selectively introduce analytes at a specific position of a nanostructure and to compare the SERS signal to that when analytes are deposited at a different position of another nanostructure of identical dimensions. Herein we demonstrate the controlled and localized deposition of SERS-active analytes onto a hot-spot region of a SERS substrate using a modified electron beam induced deposition (EBID) method.[19] The substrate consists of nanoslit cavity structures coated with a gold film.[20] SERS intensity detected from analytes deposited at different positions along the nanoslit cavities show directly that the SERS hot spot in the nanoslit is highly spatially localized, in excellent agreement with theoretical predictions. Furthermore, a kinetic model of near-field photon degradation of Raman analytes is also discussed.

EBID is a process that is usually conducted in the vacuum chamber of a scanning electron microscope (SEM) in the presence of a gas precursor (as shown in Figure 1 a). Solid material can be locally deposited onto substrates by means of electron beam mediated chemical decomposition of the precursor.[21] The modified EBID method employed herein is an easy and cheap way to deposit amorphous carbonaceous nanoparticles (CNPs) on a substrate using hexadecane as the gaseous precursor. As shown on the right of Figure 1 a, the CNPs were selectively deposited at various locations on nanoslit cavity substrates as Raman reporters. Figure 1 b shows an energy-filtered TEM (EFTEM) cross-sectional image of a CNP deposited inside the nanoslit (a carbon filter was used for this image, and the bright region in the gap is the CNP).

The Au nanoslit cavity substrate was prepared by KOH anisotropic etching of the top silicon layer in a silicon-on-insulator (SOI) wafer, resulting in a fixed opening angle (70.5°).[19,20] After coating with a 100 nm Au layer by means of sputtering, the resulting nanoslit gap was about 15 nm, with an estimated curvature at the edges of 5 nm. The nanoslit gap is well controlled (±2 nm) along the length of the slit (6 μm)

[*] C. Chen, Dr. F. Clemente, R. Kox, Prof. L. Lagae, Prof. G. Borghs, Dr. P. Van Dorpe
IMEC vzw., Kapeldreef 75, Leuven, 3001 (Belgium)
Fax: (+32) 1628-1097
E-mail: chang.chen@imec.be
pol.vandorpe@imec.be
Dr. J. A. Hutchison, Dr. H. Uji-I, Prof. J. Hofkens, Prof. G. Maes
Department of Chemistry, Katholieke Universiteit Leuven
Celestijnenlaan 200 F, 3001 Leuven (Belgium)

[**] C.C. thanks the SBA for a scholarship, P.V.D. thanks the FWO for a fellowship.

Supporting information for this article is available on the WWW under http://dx.doi.org/10.1002/anie.200905389.

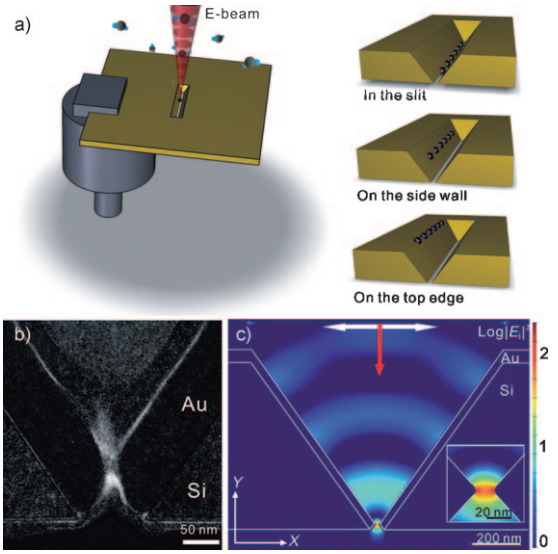

Figure 1. a) Schematic illustration of the modified EBID process with a few gas precursor molecules, and various deposition locations of CNPs. b) EFTEM image of the cross-section of a CNP (bright region) in the nanoslit. c) FDTD-simulated profile of the optical field enhancement $|E_i|^2$ distribution in a nanoslit cavity; the inset shows the $|E_i|^2$ distribution profile inside the nanoslit, showing the hot spot localized at the nanoslit. The red and white arrows indicate the direction and the polarization, respectively, of a planar light source.

and, importantly, is also maintained consistently from one nanoslit cavity structure to another.

Previously, two-dimensional numerical simulations based on the finite difference time domain technique (FDTD) were applied to obtain a simulated optical field (enhancement) distribution during optical illumination of this substrate.[20,22] These studies predicted that SP standing waves between the top and bottom convex edges of the cavity couple at the nanoslit to generate a strongly enhanced and highly localized field. The simulated field enhancement profile (Figure 1c) clearly indicates that the field is localized inside the 15 nm wide nanoslits. The field enhancement ($|E_i|^2$) was approximately 250 near the edge and about 60 at the center of the nanoslit. As the SERS enhancement factor EF scales roughly with $|E_i|^4$, the localization of the field generates an even stronger localization of the SERS signal. Based on the field distribution profile (as shown in Figure S1 in the Supporting Information), we can estimate that the vertical spatial resolution of the SERS hot spot is about 2 nm near the edge and about 4 nm at the center of the nanoslit and that the high-enhancement region is contained within a $15 \times 4\ nm^2$ area. This huge spatial inhomogeneity is comparable to or greater than that predicted for nanoparticle aggregate systems[23] and other nanoslit[24] substrates.

Experimentally the nanoslit cavity structures showed strong SERS enhancement under optical excitation after chemisorption of a sub-monolayer of Raman reporters.[20] However, as emphasized above, the relative contribution of molecules on the side wall and top edges of the cavity and those at the nanoslit cannot easily be resolved in such experiments. The relative coverage of analyte in these three regions is not known, and furthermore the distance between the nanoslit and the cavity edge (ca. 450 nm) is on the order of the diffraction limit, so scattering from the different areas cannot be resolved optically.

To demonstrate directly the spatial localization of the SERS hot spot in this structure, we deposited the CNPs inside the nanoslit, on the side wall, and at the top edge of the cavity of three nanoslit cavity structures (Figure 2a). In the latter two structures, the CNPs were deposited (225 ± 5) nm and (450 ± 5) nm away from the nanoslit, respectively. The diameter of the CNPs was about (20 ± 2) nm inside the nanoslit and (30 ± 2) nm on the side wall, and the number of particles deposited in the illumination area was roughly equivalent in each case. Raman imaging based on a band-filter-equipped CCD camera and 633 nm wide field laser illumination was used to observe SERS from the nanoslit cavity structures.[25] As shown in Figure 2b, strong and bright scattering was only observed from the structure in which the CNPs were deposited directly at the nanoslit. The corresponding SERS spectra obtained by focused illumination of

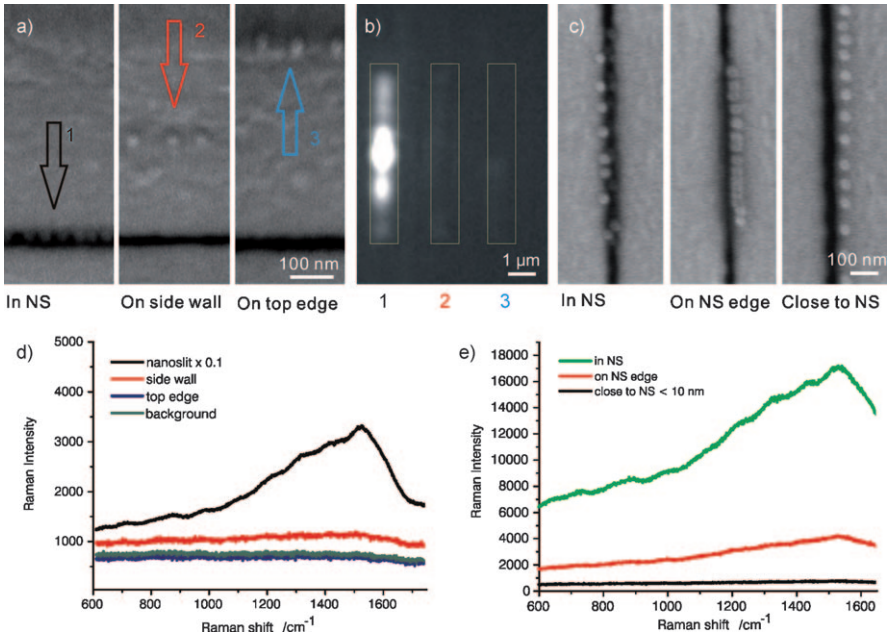

Figure 2. Distribution of SERS enhancement. a) SEM images of CNPs deposited 1) inside the nanoslit, 2) on the side wall, and 3) the top edge of the nanoslit cavity. b) Raman images of locations corresponding to those in (a); the yellow frames indicate nanoslit cavities. c) SEM images of the CNPs deposited inside the nanoslit, on the edges of the nanoslit, and very close to the nanoslit (less than 10 nm away). d) Raman spectra taken at nanoslit cavities with CNPs deposited at the different locations shown in (a). e) Raman spectra taken at nanoslit cavities with CNPs deposited at the different locations shown in (c). The integration time for the spectra was 10 s, and the spectra were accumulated three times.

this structure are shown in Figure 2d. The broad Raman band from 1100–1600 cm^{-1} was a mixture of the G band (1550–1580 cm^{-1}) and the D band (1300–1450 cm^{-1}) of amorphous carbon, corresponding to the atomic displacement of E_{2g2} and the breathing mode with A_1g symmetry only active in the presence of disorder.[26,27]

The large distinction between SERS intensities from CNPs deposited at the nanoslit compared to other locations in the nanoslit cavity structure shows directly that the SERS hot spot is localized at the nanoslit region, in line with the simulations (Figure 1c). The SERS intensity from the CNPs at the top edges of the cavity was similar to the background noise from a nanoslit cavity without CNPs, while the signals from CNPs on the side walls were slightly stronger for both the carbonaceous Raman band and the background noise. This result is also consistent with the simulations (Figure 1c), which predict a weak enhancement at the cavity wall generated by SP standing waves.

For a finer demonstration of the spatial inhomogeneity of SERS near the nanoslit, 15 CNPs as a group were deposited inside the nanoslit (Figure 2c), on the edge, and less than 10 nm away from the edge of the nanoslit of three nanoslit cavities. The corresponding Raman spectra are shown in Figure 2e. As expected, the SERS intensity decreases dramatically with increasing distance between CNPs and the nanoslit, indicating that the high SERS enhancement region is indeed confined to within 10 nm of the nanoslit. These experiments show the huge potential of EBID for detailed mapping of SERS hot spots,[6] particularly as the minimum size of EBID-fabricated nanodots was recently pushed down to 3 nm.[28]

The excitation laser exposure time, leading to photodegradation of the CNPs, provides further evidence for the high spatial localization of the SERS hot spot in the nanoslit cavity. Amorphous carbon can be decomposed under laser irradiation in a photochemical reaction, thus leading to the formation of gaseous products such as carbon dioxide, hydrocarbons, and hydrogen.[29]

For SERS studies of CNPs, a similar dependence of the decomposition rate on the localized optical field strength is expected: molecules closer to a hot spot should decompose faster,[30] and multiorder decay kinetics might occur in high-enhancement regions. Equation (1) was deduced to express the multiorder logarithmic reaction-rate model in terms of the measured SERS intensity (I_{SERS}) from a CNP experiencing an average optical field enhancement $\overline{E_i}^2$ depending on its position on the substrate during irradiation. In Equation (1), k is a standard reaction constant, P_0 is an excitation power density, A is a constant related to an activation energy of the reaction and a degradation time of molecules, n is a reaction order, t is an irradiation time, and C is a term related to the field-enhancement factor and the size of CNPs. Equation (1) predicts that the spectral intensity $\ln(I_{SERS})$ decays linearly with the nth root of time $\sqrt[n]{t}$, and that the decay rate depends on the field enhancements.

$$\ln(I_{SERS}) \approx -\sqrt[n]{k_0 e^{\left(\frac{-A}{P_0 \overline{E_i}^2}\right)}}\sqrt[n]{t} + C \qquad (1)$$

Figure 3a shows the SERS intensity as a function of time for CNPs deposited at the nanoslit, on the nanoslit edge, and 30 nm from the nanoslit. The simplest model that could adequately fit the decay data for all three CNP deposition positions was that for a second-order reaction ($n = 2$; see the Supporting Information for details).

The intention of this analysis is to obtain slopes from the decomposition curves of CNPs at different locations on the substrate that contain reliable information on the field enhancement at each location. We imported the FDTD-simulated average field enhancement factors $\overline{E_i}^2$ into the slope term in Equation (1) for a CNP at each of the three studied substrate positions and compared the ratios of the simulated slopes with those obtained from the SERS experiments (Figure 3a), finding excellent agreement (see the Supporting Information for details). Further study testing this kinetic model on different systems or reactions with known reaction order will be needed to fully understand it. Furthermore, using the rate of photoinduced decomposition of the CNPs to map the SERS enhancement distribution may be advantageous over the two methods already outlined above,[6,18] because it does not rely on absolute intensity measurements.

A final piece of evidence for the high spatial localization of the SERS enhancement in the nanoslit cavity comes from the study of the morphology of CNPs in the nanoslit during laser exposure. As the high-enhancement region in the nanoslit is much smaller than the CNP size, efficient decomposition is only expected to occur inside the CNPs and would

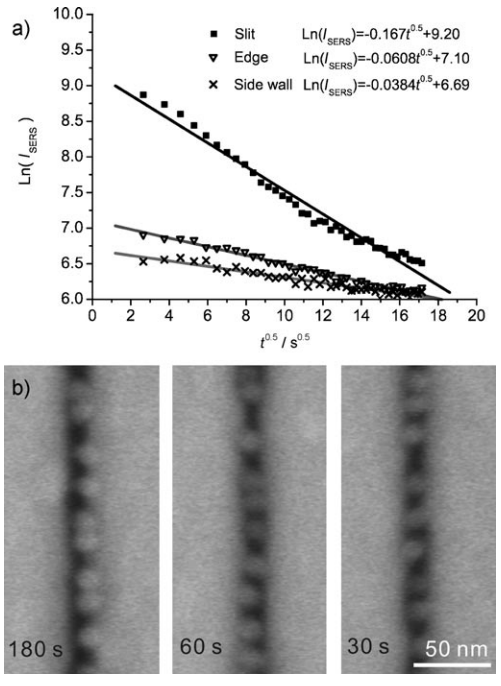

Figure 3. Near-field photon degradation of CNPs under laser illumination. a) The linear relationship between $\ln(I_{SERS})$ and the square root of time for CNPs at different locations of nanoslit cavities: inside the nanoslit (■), on the edge (▼), and 30 nm away from the nanoslit (×); the black lines are linear fits to the data. b) SEM images of CNPs inside nanoslits irradiated for 180, 60, and 30 s (from left to right).

not affect the CNP surface morphology. Indeed, the morphology of CNPs irradiated for different lengths of time did not show any obvious changes (Figure 3b). The size of the CNPs was still approximately 20 nm, independent of the laser exposure time. Additionally, as the hot spot is smaller than the CNP, the SERS intensity should scale linearly with the CNP diameter. This is exactly what we observe (Figure S4 in the Supporting Information), giving more evidence for the high spatial localization.

In summary, we used position-selective EBID of CNPs to obtain direct evidence for the high spatial localization of the SERS hot spots in a nanoslit cavity substrate. The experiments confirm the predictions of FDTD simulations and demonstrate that the nanoslit cavity is a high spatial resolution substrate for SERS spectroscopy. Controlled deposition of CNPs along substrates allows the SERS hot spot to be mapped directly. For this method, small particles and very high spatial control are obviously desirable. An additional estimate of hot-spot localization may be obtained by controlling the amount of material deposited at a single site on a substrate. Thirdly, we showed that the rate of degradation of CNPs' SERS signals correlates with the theoretical field enhancement as a function of position in a hot-spot region, offering a third way to map the hot-spot distribution that is not reliant on absolute SERS intensity values. We believe the techniques outlined above will be very useful for both probing the spatial distribution of SERS hot spots on broad a range of substrates (e.g. nanoparticle dimers, nanorings, nanowires) and for studying near-field photochemical reactions.

Experimental Section

The nanoslit cavity substrates were fabricated by standard micromachining techniques on a SOI wafer.[19] In brief, electron-beam lithography combined with KOH wet etching were used to form the nanoslit cavities on freestanding Si membranes. Then a gold layer was deposited by a sputtering process, resulting in a gold nanoslit cavity with a size of about (15 ± 2) nm and a length of 6 μm.

A custom-built gas injection system for introducing hexadecane as the precursor was used in EBID (Figure 1a). EBID was operated in a SEM (Philips, XL30 FESEM) at a 10 kV accelerating voltage and a 160 μA emission current with a beam spot size of 2. CNPs were deposited manually by spot modes in SEM. The average size of the obtained CNPs was about (20 ± 2) nm inside the nanoslits. The placing accuracy of the CNPs was approximately 5 nm. In SERS measurements (LabRAM HR from Hobiba Scientific, Ltd and a custom-built Raman system), the number of CNPs under laser illumination (632.8 nm) was the same in each sample. The integration time for the spectra was 10 s, and spectra were accumulated three times for each measurement. In the laser exposure time experiments, the integration time was 5 s, the step time was 7 s, and the total process time was approximately 300 s.

A focused ion beam SEM (FIB-SEM; FEI, Strata 400 STEM) and an energy-filtered transmission electron microscope (EFTEM, Tecnai F30, FEI, operating at 300 kV) were used to make the cross section of the sample and to characterize CNPs. All SEM and TEM images were taken after SERS measurements.

See the supporting information for further experimental details.

Received: September 25, 2009
Published online: November 20, 2009

Keywords: hot spots · localization · nanotechnology · photochemistry · Raman spectroscopy

[1] Z. Loffe, T. Shamai, A. Ophir, G. Noy, I. Yutsis, K. Kfir, O. Cheshnovsky, Y. Selzer, *Nat. Nanotechnol.* **2008**, *3*, 727.
[2] B. D. Moore, L. Stevenson, A. Watt, S. Flitsch, N. J. Turner, C. Cassidy, D. Graham, *Nat. Biotechnol.* **2004**, *22*, 1133.
[3] S. M. Nie, S. R. Emory, *Science* **1997**, *275*, 1102.
[4] E. C. Le Ru, P. G. Etchegoin, *Principles of Surface-Enhanced Raman Spectroscopy and Related Plasmonic Effects*, Elsevier, Oxford, **2009**.
[5] E. Hao, G. C. Schatz, *J. Chem. Phys.* **2004**, *120*, 357.
[6] Y. Fang, N. H. Seong, D. D. Dlott, *Science* **2008**, *321*, 388.
[7] P. G. Etchegoin, E. C. Le Ru, *Phys. Chem. Chem. Phys.* **2008**, *10*, 6079.
[8] E. C. Le Ru, P. G. Etchegoin, M. Meyer, *J. Chem. Phys.* **2006**, *125*, 204701.
[9] D. A. Genov, A. K. Sarychev, V. M. Shalaev, A. Wei, *Nano Lett.* **2004**, *4*, 153.
[10] J. Ye, P. Van Dorpe, W. Van Roy, G. Borghs, G. Maes, *Langmuir* **2009**, *25*, 1822.
[11] P. Gadenne, X. Quelin, S. Ducourtieux, S. Gresillon, L. Aigouy, J. C. Rivoal, V. Shalaev, A. Sarychev, *Physica B* **2000**, *279*, 52.
[12] J. Nelayah, M. Kociak, O. Stephan, F. J. G. De Abajo, M. Tence, L. Henrard, D. Taverna, I. Pastoriza-Santos, L. M. Liz-Marzan, C. Colliex, *Nat. Phys.* **2007**, *3*, 348.
[13] E. C. Le Ru, P. G. Etchegoin, *Chem. Phys. Lett.* **2004**, *396*, 393.
[14] B. Pettinger, B. Ren, G. Picardi, R. Schuster, G. Ertl, *Phys. Rev. Lett.* **2004**, *92*, 096101.
[15] A. Hartschuh, E. J. Sanchez, X. S. Xie, L. Novotny, *Phys. Rev. Lett.* **2003**, *90*, 095503.
[16] J. A. Dieringer, A. D. McFarland, N. C. Shah, D. A. Stuart, A. V. Whitney, C. R. Yonzon, M. A. Young, X. Y. Zhang, R. P. Van Duyne, *Faraday Discuss.* **2006**, *132*, 9.
[17] S. Lal, N. K. Grady, G. P. Goodrich, N. J. Halas, *Nano Lett.* **2006**, *6*, 2338.
[18] P. H. C. Camargo, M. Rycenga, L. Au, Y. N. Xia, *Angew. Chem.* **2009**, *121*, 2214; *Angew. Chem. Int. Ed.* **2009**, *48*, 2180.
[19] R. Kox, C. Chen, G. Maes, L. Lagae, G. Borghs, *Nanotechnology* **2009**, *20*, 115302.
[20] C. Chen, J. A. Hutchison, P. Van Dorpe, R. Kox, I. De Vlaminck, H. Uji-i, J. Hofkens, L. Lagae, G. Maes, G. Borghs, *Small* **2009**, DOI: 10.1002/smll.200901312.
[21] S. J. Randolph, J. D. Fowlkes, *Crit. Rev. Solid State* **2006**, *31*, 55.
[22] N. M. B. Perney, F. J. G. de Abajo, J. J. Baumberg, A. Tang, M. C. Netti, M. D. B. Charlton, M. E. Zoorob, *Phys. Rev. B* **2007**, *76*, 035426.
[23] K. Kneipp, Y. Wang, H. Kneipp, L. T. Perelman, I. Itzkan, R. Dasari, M. S. Feld, *Phys. Rev. Lett.* **1997**, *78*, 1667.
[24] X. D. Chen, A. B. Braunschweig, M. J. Wiester, S. Yeganeh, M. A. Ratner, C. A. Mirkin, *Angew. Chem.* **2009**, *121*, 5280; *Angew. Chem. Int. Ed.* **2009**, *48*, 5178.
[25] J. A. Hutchison, S. P. Centeno, H. Odaka, H. Fukumura, J. Hofkens, H. Uji-i, *Nano Lett.* **2009**, *9*, 995.
[26] A. C. Ferrari, J. Robertson, *Phys. Rev. B* **2000**, *61*, 14095.
[27] J. Robertson, *Mater. Sci. Eng. R* **2002**, *37*, 129.
[28] L. Van Kouwen, A. Botman, C. W. Hagen, *Nano Lett.* **2009**, *9*, 2149.
[29] L. H. Zhang, H. Gong, J. P. Wang, *J. Appl. Phys.* **2002**, *92*, 2962.
[30] P. G. Etchegoin, E. C. Le Ru, R. C. Maher, L. F. Cohen, *Phys. Chem. Chem. Phys.* **2007**, *9*, 4923.

